

Implementing feature binding through dendritic networks of a single neuron

Yuanhong Tang[†], Shanshan Jia[†], Tiejun Huang[†], Zhaofei Yu[†], Jian K. Liu[‡]

[†]School of Computer Science, Institute for Artificial Intelligence, Peking University, Beijing, China

[‡]School of Computer Science, Centre for Human Brain Health, University of Birmingham, Birmingham, UK

Abstract

A single neuron receives an extensive array of synaptic inputs through its dendrites, raising the fundamental question of how these inputs undergo integration and summation, culminating in the initiation of spikes in the soma. Experimental and computational investigations have revealed various modes of integration operations that include linear, superlinear, and sublinear summation. Interestingly, distinct neuron types exhibit diverse patterns of dendritic integration contingent upon the spatial distribution of dendrites. The functional implications of these specific integration modalities remain largely unexplored. In this study, we employ the Purkinje cell as a model system to investigate these intricate questions. Our findings reveal that Purkinje cells (PCs) generally exhibit sublinear summation across their expansive dendrites. The degree of sublinearity is dynamically modulated by both spatial and temporal input. Strong sublinearity necessitates that the synaptic distribution in PCs be globally scattered sensitive, whereas weak sublinearity facilitates the generation of complex firing patterns in PCs. Leveraging dendritic branches characterized by strong sublinearity as computational units, we demonstrate that a neuron can adeptly address the feature-binding problem. Collectively, these results offer a systematic perspective on the functional role of dendritic sublinearity, providing inspiration for a broader understanding of dendritic integration across various neuronal types.

I. INTRODUCTION

Neurons, the foundational computational entities within the intricate brain system, intricately process signal inputs received through their dendritic spine. Conventional understanding of dendritic function posits that these structures receive synaptic input and subsequently convey it to the soma, thus initiating the generation of action potentials or spikes. This proposition suggests that a single neuron possesses computational capabilities to execute information processing through an extensive array of dendritic branches. However, the underlying integrating principles

governing the diverse array of dendrites and neuron types remain elusive. In recent decades, experimental studies have facilitated laborious explorations of the integration of synaptic inputs along the dendritic domains of individual neurons, shedding light on the physiological basis of dendrite function [1], [2], [3], [4]. Dendrites have been shown to function as autonomous information processing units, capable of performing local computations, thus conferring substantial computational capabilities on single neurons [5], [6], [7], [8], [9], [10]. Furthermore, these insights have significantly contributed to our understanding of how neurons engage in communication with one another and the resultant impact on behavior [11], [12], [13], [14].

The principal function of dendrites lies in the intricate integration and processing of synaptic inputs [6], [15]. Investigations focusing on pyramidal cells reveal that dendritic integration is characterized by superlinear dynamics, attributed to the activation of voltage-dependent channels and NMDARs [12], [16], [17], [18]. In particular, this superlinear integration has been observed primarily in cortical neurons [11], [19], [20], while sublinear summation has been documented in cerebellar interneurons [21], [22]. The manifestation of dendritic nonlinearity allows neurons to function as feature detectors [14], [13], exerting influence on various aspects of brain function, including whisker sensation [23], orientation selectivity [24], sensory perception [25], [26], sensory-motor integration [23], and memory encoding [27], [28]. Furthermore, nonlinear dendritic integration is postulated to augment the computational capacity of neurons [29], [30], enabling them to compute linearly non-separable functions [31], [32]. The incorporation of nonlinear dendritic mechanisms into artificial neural networks is proposed to bring neurons in comparative alignment with their biological counterparts [33], [34], [28], [5]. The benefit of installing dendritic nonlinearity into artificial neural networks not only reduces power consumption and enhances accuracy [35], [36] but also mitigates communication costs within neural networks [37].

The majority of investigations into dendritic nonlinearity have predominantly centered on cortical neurons. However, there is a substantial gap in our understanding of the dendritic nonlinearity inherent in the most complex neuronal entities, namely cerebellar Purkinje cells (PCs) [38]. The intricate dendritic structures of PCs contribute to amplification of the computational repertoire within single neurons. PCs, characterized by receiving thousands of synaptic inputs in a location-dependent manner, exhibit a distinctive synaptic organization, with the distal region of the dendritic tree receiving excitatory input from parallel fibers originating from granule cells [39]. On the contrary, the proximal portion of the dendritic tree is innervated by the

input of climbing fibers [40]. The interplay between synaptic input and dendritic nonlinear properties produces highly intricate input-output functions [34]. Therefore, it is imperative to understand whether passive cable properties contribute to location-dependent dendritic integration and whether dendritic synaptic integration plays a role in PC computation.

In this study, we employ detailed PC models that capture the intricacies of dendritic morphology to investigate dendritic nonlinear synaptic integration and its implications in information processing. Our examination of subthreshold synaptic summation in PCs reveals a significant sublinear synaptic integration profile. Notably, the strong sublinearity of spiny dendrites necessitates that PC have globally scattered inputs to fire somatic spikes. Furthermore, we observe that weak sublinear responses in smooth dendrites promote the generation of bursts, potentially leading to the generation of complex spikes. From the perspective of dendritic nonlinearity, this explains why the synaptic distribution in Purkinje cell is location-dependent. Importantly, this sublinearity enables a single neuron to compute feature binding problems. Our results suggest that while nonlinear dendrites may not supplant neurons as the fundamental computational units, they undoubtedly expand the computational capacities of neuronal systems.

II. METHODS

A. Neuronal model

In this study, we employed a detailed neuron model incorporating neuromorphic structures to explore the dendritic nonlinear synaptic integration capabilities of Purkinje cells and how dendritic nonlinearity affects neuronal response and computational capabilities. This model extends the traditional Hodgkin-Huxley framework by including detailed representations of the neuron's morphology, such as dendrites and soma compartments, to better capture the spatial and temporal dynamics of electrical signaling. The Hodgkin-Huxley model describes the membrane potential V through a set of nonlinear differential equations. These equations account for the ionic currents across the neuronal membrane, and leakage currents. In the neuromorphic model, these equations are applied to multiple compartments representing different parts of the neuron. The membrane potential dynamics for each compartment i are given by:

$$C_m \frac{dV_i}{dt} = -I_{\text{ion},i} - I_{L,i} + I_{\text{syn},i} + \sum_j \frac{g_{ij}}{C_m} (V_j - V_i) \quad (1)$$

where C_m is the membrane capacitance, $I_{ion,i}$ is the ion current in compartment i , $I_{L,i}$ is the leakage current in compartment i , $I_{syn,i}$ is the synaptic current applied to compartment i , g_{ij} is the conductance between compartments i and j , V_j is the membrane potential of compartment j .

Ion channels are fundamental components of the neuronal membrane, responsible for generating and propagating electrical signals in neurons. In this study, we modeled the behavior of these ion channels using the Hodgkin-Huxley framework. This framework provides a detailed biophysical description of how these ion channels contribute to the membrane potential dynamics. The ion current I_{ion} is given by:

$$I_{ion} = g_{ion} m^n h^i (V - E_{ion}) \quad (2)$$

where: g_{ion} is the maximum ion conductance, m is the activation gating variable, h is the inactivation gating variable, n and i represent the number of activation and inactivation gates respectively, V is the membrane potential, E_{ion} is the ion reversal potential. The gating variables m and h follow first-order kinetics with voltage-dependent rate constants:

$$\begin{aligned} \frac{dm}{dt} &= \alpha_m(1 - m) - \beta_m m \\ \frac{dh}{dt} &= \alpha_h(1 - h) - \beta_h h \end{aligned} \quad (3)$$

where $\alpha_{m,h}$ and $\beta_{m,h}$ are rate constants for the ion channel. I_L is the leakage ion channel represents the passive flow of ions through the membrane, contributing to the resting membrane potential. The leakage current I_L is given by:

$$I_L = g_L(V - E_L) \quad (4)$$

where: g_L is the leakage conductance, V is the membrane potential, E_L is the leakage reversal potential.

We used a 3D reconstruction of a mouse Purkinje cell available on the public archive www.neuromorpho.org (NMO-00865). The model contains a somatic compartment and 739 dendrites. The PC was modeled with the same parameters as before [41]. Membrane resistance (R_m) and axial resistance (R_i) were uniformly set to $5000\Omega/\text{cm}^2$ and $250\Omega/\text{cm}$, respectively. Membrane capacitance (C_m) was set to $0.8\text{F}/\text{cm}^2$ in soma and main dendrites, and $1.5\text{F}/\text{cm}^2$ in spiny dendrites. 13 different types of voltage-gated ion channels were installed in the PC model. Three ion channels (fast Na^+ channel, persistent Na^+ channel, anomalous rectifier channel) were solely added to the soma, and two ion channels (high-threshold Ca^{2+} -activated K^+ channel, low-threshold Ca^{2+} -activated K^+

channel) were solely added to the dendrites. Eight of which (P-type Ca^{2+} channel, T-type Ca^{2+} channel, class-E Ca^{2+} channel, persistent K^+ channel, A-type K^+ channel, D-type K^+ channel, delayed rectifier, decay of sub-membrane Ca^{2+}) were inserted into the soma and dendrites.

B. Synapse model

Synapses are critical structures that mediate communication between neurons through the release of neurotransmitters. The synapse models are based on the biophysical properties of synaptic currents and their interaction with the postsynaptic membrane. In this study, to explore the dendritic nonlinear synaptic integration ability of PCs, we established two excitatory synapse models: AMPA and NMDA. Excitatory synapses typically involve the release of neurotransmitters such as glutamate, which bind to receptors on the postsynaptic neuron, leading to depolarization. The excitatory postsynaptic current (EPSC) can be represented by a mathematical as:

$$\begin{aligned} I_{syn} &= g_{syn} * (V - E_{syn}) \\ g_{syn} &= g_{max} * w * Y * s \end{aligned} \quad (5)$$

I_{syn} is the receptor current, g_{syn} is the receptor conductance, V is the membrane potential, E_{syn} is the receptor reversal potential, g_{max} is the maximum synaptic conductance, w is the connection weight between the synaptic stimulus and the neuron. NMDA-mediated currents often require AMPA-mediated depolarization to remove extracellular Mg^{2+} blockade of NMDA-associated channels, the associated channels open only when magnesium ions are blocked and NMDA receptors are activated. Therefore the scaling factor Y was:

$$\begin{cases} Y = 1/(1 + 0.24 * \exp(-154 * v/0.027)) \text{ for NMDA} \\ Y = 1 \text{ for AMPA} \end{cases} \quad (6)$$

The synaptic gating variable s follows double exponential kinetics:

$$s(t) = e^{-(t-t_{spike})/\tau_{decay}} - e^{-(t-t_{spike})/\tau_{rise}} \quad (7)$$

where τ_{rise} is the rise time constant, τ_{decay} is the decay time constant, and t_{spike} represents the time of the presynaptic spike, and rise time constant τ_{rise} was set 0.5 ms, 8 ms for AMPA and NMDA, and decay time constant τ_{decay} was set 5 ms, 30 ms for AMPA and NMDA, respectively. When the excitatory synapse includes both an AMPA and an NMDA component, they are co-located and always co-activated. When calculating dendritic nonlinearity, synapses are distributed

starting at the 0.1 position of the dendrite, then added distally at intervals of $d = 0.2$ from the starting point.

Each synapse received an independent spike train generated as a stimulus input. A single stimulation consists of a sequence of spikes containing spike times and inter-spike intervals, so we can generate a successive spike train by the previous spike plus the regular or irregular time intervals. In this study, we utilized a Poisson-distributed pulse sequence model to investigate the response of neurons to stochastic external stimuli. The spike train was generated according to a Poisson process, characterized by an average firing rate λ (pulses per second). The intervals between pulses, Δt , were exponentially distributed with parameter λ , ensuring that the pulse arrivals are memoryless and randomly timed. The probability density function of the inter-pulse intervals is given by:

$$P(\Delta t) = \lambda e^{-\lambda \Delta t} \quad (8)$$

where Δt is the time between consecutive pulses. Firstly, we generate a random number u uniformly distributed in the interval $(0, 1)$. Then compute the inter-pulse interval Δt using the inverse transform sampling method:

$$\Delta t = -\frac{1}{\lambda} \ln(1 - u) \quad (9)$$

and the next pulse arrival time is $t_{i+1} = t_i + \Delta t$ and this process was repeated to generate a sequence of pulse arrival times over the desired simulation period.

In this study, we examined the effects of both synchronous and asynchronous inputs on neuronal activity. Synchronous inputs involve multiple synapses receiving input pulses simultaneously which can lead to a strong and coordinated response in the postsynaptic neuron. Asynchronous inputs involve multiple synapses receiving input pulses at different times, leading to a more distributed and less coordinated response in the postsynaptic neuron.

C. Data analysis

We simulated the PC morphology model in NEURON 8.4. The time step of all simulation experiments was set at 0.025ms. Data collected after simulations was saved for further analysis. In order to avoid the influence of ionic current on the nonlinear synaptic integration ability of dendrites, there is no ion channel distribution in all compartments of PC when calculating dendritic nonlinearity. To study dendritic nonlinearity, we record observed EPSPs (EPSP_O)

and the EPSPs produced by individual synapses are added together to obtain the expected EPSP ($EPSP_E$). The sublinearity index was measured as the average sublinear summation $(1 - (EPSP_O/EPSP_E)) * 100$ with the last two points as in the dash box in Figure 1. To investigate the temporal dependence of dendritic integration, we systematically varied the interspike intervals (ISI) between synaptic inputs. Then, the amplitude of all EPSPs induced by the stimuli was averaged to obtain the EPSP value elicited by the stimulus. From this, the observed values and expected values were obtained, and the sublinearity index was calculated.

In addition, the expected and observed EPSP curves are fitted by the Hill function as previously [42]:

$$F(EPSP_E) = \frac{EPSP_{Omax}}{1 + (EPSP_{E50}/EPSP_E)^n} + EPSP_{O0} \quad (10)$$

where n is the exponent factor, $EPSP_{O0}$ the observed EPSP offset, and $EPSP_{Omax}$ the maximum observed EPSP. $EPSP_{E50}$ is the value of expected EPSP at which observed EPSP reaches half maximum. To characterize EPSP in detail, we introduced three measures, the peak, rise time, and width of EPSP. Peak is the maximum peak value of EPSP, and width as the distance between the points where the half-amplitude reaches before and after the peak.

In order to further study the effect of dendritic nonlinearity on PC firing. The dendrites with less than 20% sublinearity are regarded as main dendrites, and those with more than 20% are regarded as spiny dendrites, and then the spiny dendrites are divided into 24 branches, and the parent node of each branch is the main dendrite.

Feature binding refers to the brain's ability to integrate various attributes (e.g., color, shape, motion) into a coherent percept. This process involves complex, nonlinear interactions within neuronal dendrites. When there are multiple synaptic inputs I_1, I_2, \dots, I_n . The nonlinear response R can be described by a function f :

$$R = f(I_1 + I_2 + \dots + I_n) \quad (11)$$

When studying PC computing performance, each branch is considered a computing unit. When the synapses distributed on the branch are activated, the input I_n is considered to be 1, and when it is not activated, the input I_n is considered to be 0. When studying Boolean functions, choose any 2 from 24 branches as X_1 and X_2 . when studying the feature binding problem, 4 of the 24 branches are selected as $X_1, X_2, X_3,$ and X_4 .

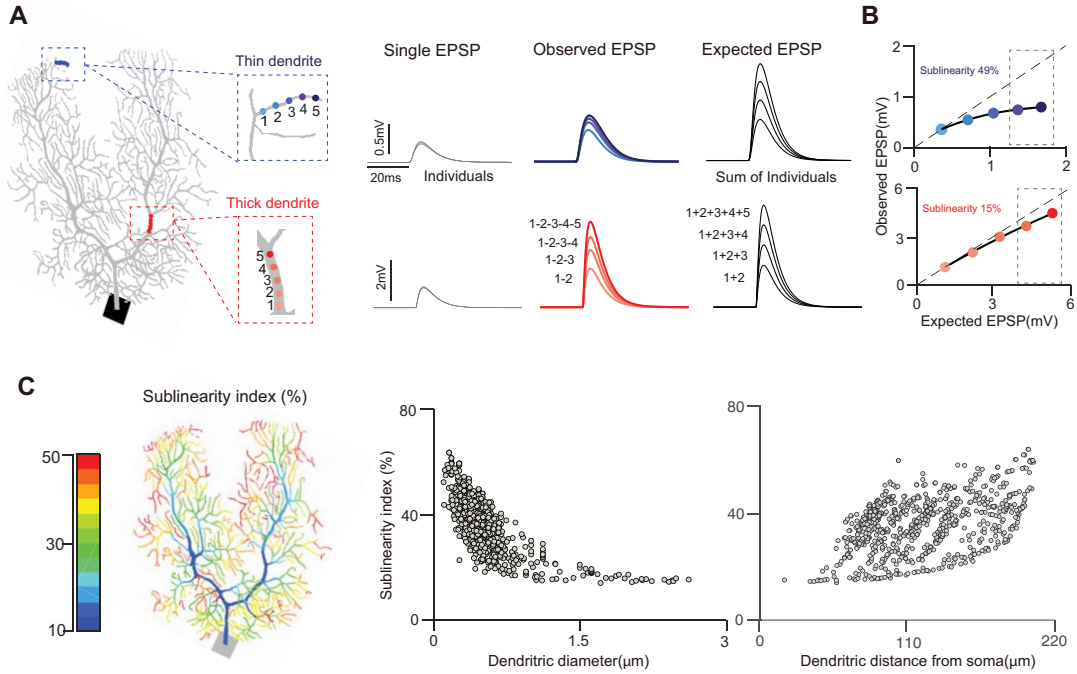


Fig. 1: PC individual dendrites show sublinear integration to the somatic response. (A) (Left) 5 synapses are distributed on thin (blue) and thick (red) dendrites. (Right) Single EPSPs evoked by single pulse synaptic stimulation; Observed EPSPs evoked with increasing synapses; Expected EPSPs as the algebraic sum of single EPSPs. (B) Sublinear relationship of the expected and observed EPSPs from (A). Dotted line represents linear function. The sublinearity index, 49% (thin) and 15% (thick) was measured as the average sublinear summation in the dashed box. Solid line indicates fits by Hill function. (C) The distributed sublinearity index for each dendrite. Sublinearity as a function of dendritic diameter and distance from soma.

III. RESULT

A. PC dendrites show sublinear integration

To examine whether the large dendritic depolarization could decrease the synaptic current driving force and introduce a nonlinearity that would curtail linear summation of somatic EPSPs (excitatory postsynaptic potentials) within the same PC dendrite, we studied subthreshold input-output relationships by comparing the algebraic sum of individual EPSP from five activated synapses along different yet nearby spatial locations along one dendrite, with the compound EPSP in response to simultaneous activation of multiple 2 to 5 locations (Figure 1A). The compound EPSP observed (EPSP_O) was systematically smaller than the algebraic sum of its

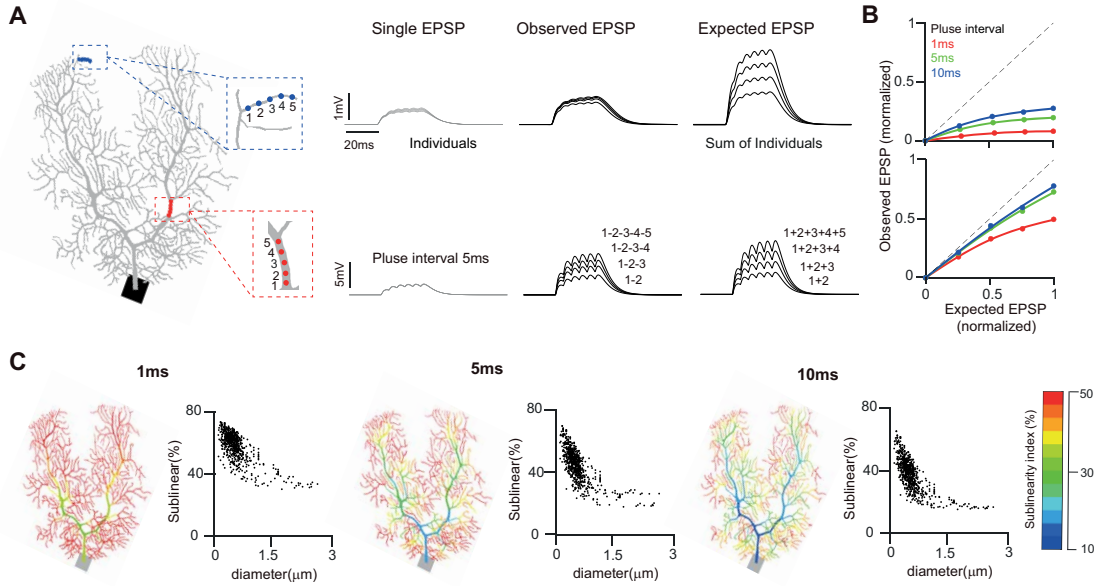


Fig. 2: Temporal dependence of sublinear dendritic integration. (A) (Left) Synapses are distributed on thin (blue) and thick (red) dendrites. (Right) Single EPSPs evoked by six-pulse synaptic stimulation; Observed EPSC with increasing synapses; Expected EPSP as algebraic sum of single EPSPs. The pulse interval is 5 ms. (B) Sublinear relationship of normalized expected and observed EPSPs at different time intervals of 1, 5, and 10 ms. The dotted line represents linear function. The solid line indicates fits by Hill function. (C) The distributed sublinearity index for each dendrite when the pulse interval is 1, 5, and 10 ms. Sublinearity as a function of dendritic diameters.

corresponding individual EPSP expected ($EPSP_E$), especially on thin dendrites. The input-output relationship of dendritic summation using these five synapses shows sublinear trends that can be fitted by the Hill function. The sublinearity index (SI) can be calculated (the average of $(1 - (EPSP_O/EPSP_E)) * 100$ using the last two points; dashed box in Figure 1B) for each dendrite. The SI of the thin dendrite (diameter $0.29\mu m$, 49%) is stronger than the thick dendrite (diameter $1.75\mu m$, 15%) as in Figure 1B. We then asked how dendritic properties regulate the SI (Figure 1C). The SI of 739 dendrites was distributed over the entire dendritic field, which shows apical dendrites exhibit stronger SIs, but trunk dendrites are weaker. SI decreases with larger diameter dendrites while increasing with the dendritic distance from the soma. Such observations are inherent in the observed and expected EPSPs (Figure S1). The peak, rise time, and width of EPSP are also location dependent (Figure S2).

To further explore the effect of temporal summation on a sequence of synaptic inputs on dendritic sublinearity, we used stimulation protocols with six temporal pluses at different intervals (1, 5, and 10 ms) with the same five spatial synaptic locations (Figure 2A). Indeed the SI can be significantly changed by temporal intervals (Figure 2B) for individual dendrites. The smaller interval can increase SI, while the larger interval reduces SI. Such a change is systematically preserved over all the dendrites (Figure 2C). For simplicity, the 5 ms interval was used throughout this study. These results suggest that PC dendritic summation shows strong sublinearity.

B. Strong sublinearity prefers a global scatter input strategy

Given that PCs typically show a significantly high firing rate and install a large number of dendrites, they receive a large number of input from Granular cells over the entire dendrite field. We then study how different spatial types of synaptic inputs can affect somatic firing through dendritic sublinearity. We selected dendrites with a sublinearity index greater than 20% as spiny dendrites and grouped them into 24 branches along the main dendrites (Figure 3A). For each branch, only one dendritic segment connects it to the parent main dendrite. To simulate clustered synaptic input, 50 synapses were distributed on a single dendrite or branch and activated synchronously. Figure 3B shows the somatic response by stimulating single dendrites (gray) and individual branches (colored) with a clustered input. Overall, the maximum membrane potential is greater when synapses are randomly distributed throughout the dendrites within a branch (scattered input) than when synapses are clustered on a single dendrite (cluster input), except for those dendrites close to the main trunk. Distance-dependent properties make proximal dendrites more responsive.

Strong dendritic sublinearity makes the somatic spiking firing threshold more difficult to reach (Figure 3C). The type of dendritic operation strongly contributes to the nature of the resultant neuronal computation. For a neuron with sublinear dendrites, clustered synaptic activity will be less efficient at triggering a spike than scattered input distributed in different dendrites due to strong sublinearity (Figure 3B). By varying the number of synaptic inputs, the input-output relationship obtained from single dendrites and the entire branch shows that the summation over multiple branches using scattered inputs can enhance the firing significantly (Figure 3D). Using branch 1 (br 1) within the left main trunk, as an example, the input-output curves of all dendrites in branch 1 in Figure 3D (left) show that the synapses are randomly distributed throughout the

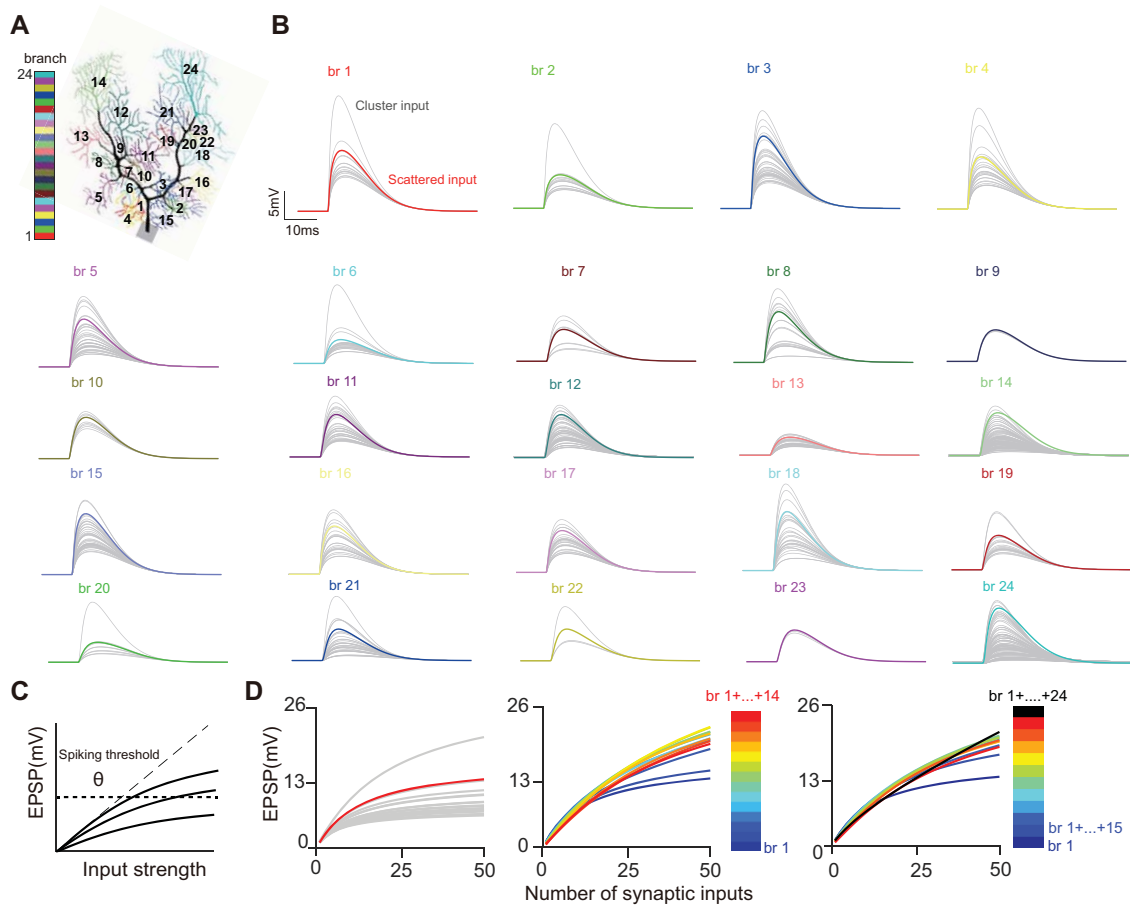


Fig. 3: Scattered synaptic inputs on strong sublinear dendrites trigger larger somatic responses. (A) 24 branches (color-coded) with strong sublinearity are segmented in the entire morphology. Each branch groups a set of single dendrites with sublinearity index $\geq 20\%$. Black trunk represents the main dendrites (dendritic sublinearity $\geq 20\%$). (B) Somatic EPSP in response to 50 synaptic inputs in a branch. Individual gray traces represent the response to a cluster input (50 synapses are distributed closely) on a single dendrite. The color trace shows synapses scattered throughout the branch. (C) Illustration of the somatic spiking threshold θ with varying degrees (solid lines) of dendritic sublinearity. Strong sublinearity makes soma voltage more difficult to reach the spiking threshold. (D) Input-output (IO) relationship curves changing over the sum of dendritic branches. (Left) IO curves in branch 1 (br1 in (B)). Gray traces represent cluster input on single dendrites. The color trace shows synapses scattered throughout the branch. (Right) IO curves obtained by scattered synaptic inputs throughout the cumulative branches on top of br1.

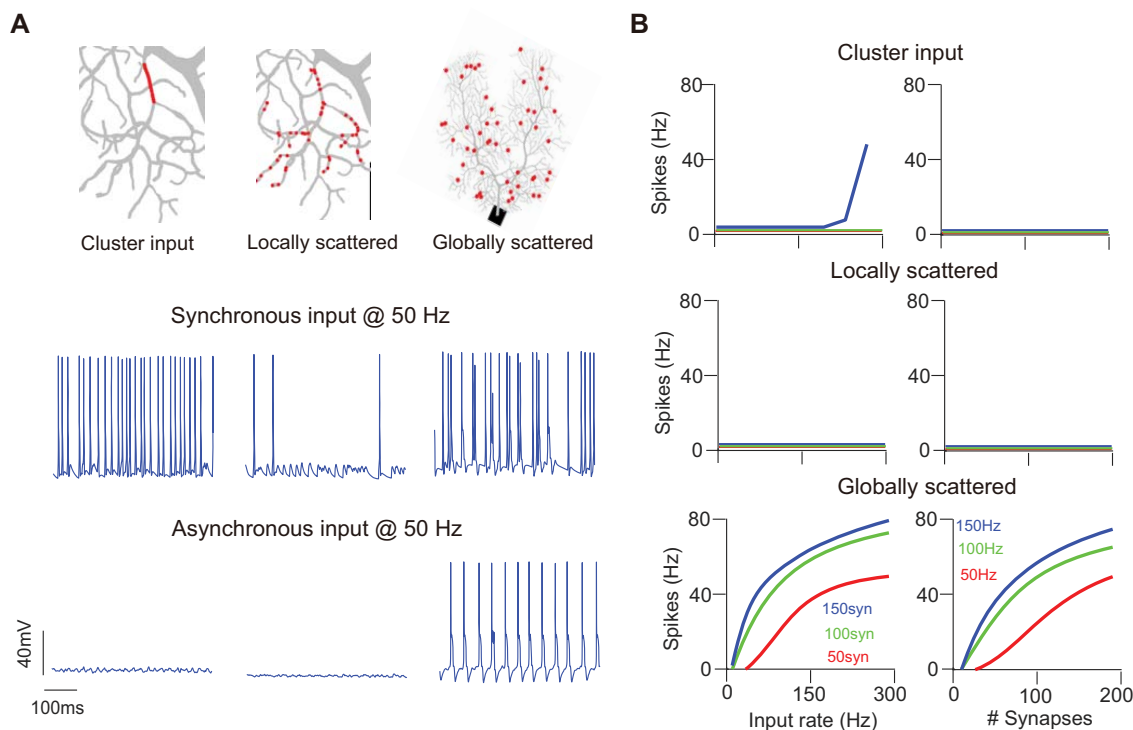


Fig. 4: Somatic spiking response boosted by globally scattered synaptic inputs across strong sublinear dendrites. (A) Spiking activity generated by synaptic inputs under three spatial and two temporal patterns. (Left) cluster input: synapses distributed in a single dendrite. (Middle) locally scattered: synapses distributed in individual branches. (Right) globally scattered: synapses distributed across all branches. Somatic spiking activity in response to either synchronous or asynchronous 50 synaptic inputs under each spatial stimulation pattern at 50 Hz. (B) Spiking activity vs. asynchronous input under three spatial stimulation patterns with (left) 50, 100, and 150 synapses; (right) 50, 100, and 150 Hz.

branch to produce a larger EPSP, except for dendrite 419 (top gray curve). Coactivation of branch1 with other branches can produce higher peak EPSP (Figure4D, middle and right).

To further examine how dendritic sublinear integration regulates somatic output under different spatial distributions, we considered three input strategies of synapses(Figure 4A, top), using dendritic 419 in branch 1, which has the highest peak of EPSP, as an example. When all 50 synapses are activated synchronously, spikes are induced in all distribution strategies, but locally scattered has fewer spikes (Figure 4A, middle). However, when synapses are activated asynchronously as the Poisson process, spikes are generated only under the global scattered

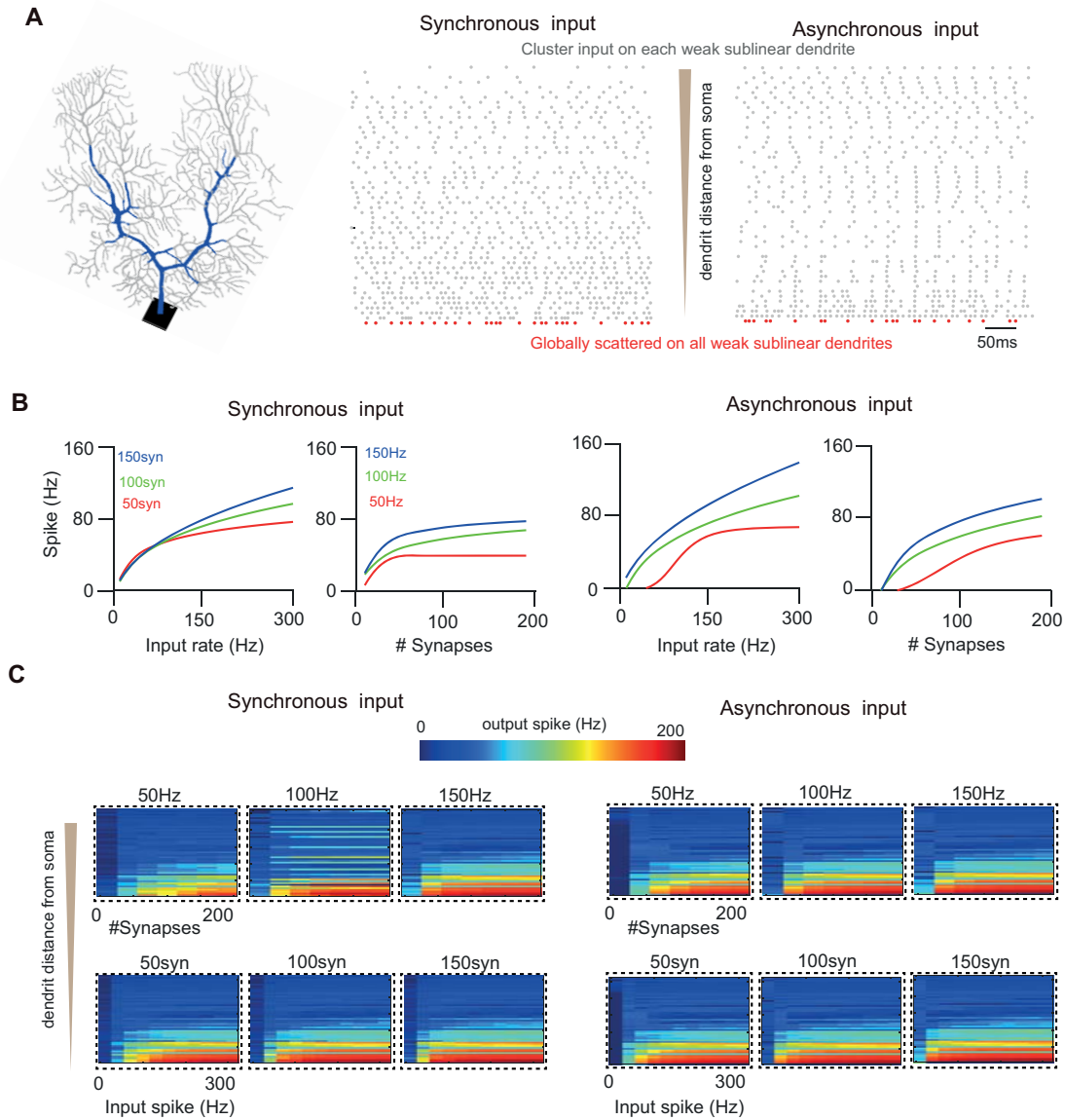


Fig. 5: Somatic spiking response is minimally affected by spatial and temporal synaptic input patterns on weak sublinear dendrites. (A) (Left) main dendrites (blue) are defined by weak sublinearity less than 20%. (Right) Raster plot of somatic spiking activity triggered by 50 synaptic synchronous and asynchronous inputs on main dendrites at 100Hz with the simulation of cluster input (gray) in each single dendrite and globally scattered (red) across all main dendrites. Each dot is a spike time. Each row in gray shows spiking in response to a single dendrite with decreasing order of dendritic distance to soma. (B) Spiking activity vs. input rate using (left) synchronous and (right) asynchronous stimulation with 50, 100, and 150 synapses or 50, 100, and 150 Hz using globally scattered synaptic inputs. (C) Similar to (B) but using cluster synaptic inputs on each single dendrite.

distribution (Figure 4A, bottom). We further increased the number of synapses and stimulation frequency and found that only the global scattered distribution induced spiking activity under asynchronous activation in branch 1 (Figure 4B). In contrast, both cluster input and locally scattered input can not effectively produce spiking. However, changing the number of synapses and stimulation frequency during synchronous activation induces spike production under all distribution strategies without selectivity (Figure S3).

The effect of sublinearity can be revealed using trunk dendrites with less than 20% sublinearity index (Figure 5A). We found that stimulation on these dendrites is more likely to induce spiking (Figure 5A), independent of synaptic temporal activation mode, synchronous or asynchronous input, as well as spatial distribution strategy, scattered (Figure 5B) or cluster (Figure 5C) input. While the closer the synaptic distribution location is to soma, the more spikes are induced. These results are consistent with the notation that climbing fibers targeting trunk dendrites close to soma can trigger more complex spikes.

C. Strong sublinearity suppress bursting spike

To examine the view that climbing fiber (CF) input induces complex spikes (CSs) in PCs, we test the potential for CSs at different dendritic locations. Figure 6A displays an example of cluster input synapses distributed at three sites. CSs as spiking bursts can not be induced by 100 synapses and can not be triggered with AMPA-like parallel fibers (PF). With 400 synapses, CSs occur in the presence of CFs with additional NMDA receptors (Figure 6B). Dendrites with weaker sublinearity and larger peaks are more likely to produce CS when CF inputs, which is relatively independent of the number of synapses (Figure 6C).

We then combined both PF and CF inputs to simulate a more realistic scenario. Background excitatory input was mimicked by distributing PF synapses evenly onto spiny dendrites at 30 Hz, and CF inputs were mimicked by distributing synapses onto the different sublinear regions with different numbers of synapses (Figure 6D). With 200 synapses, complex spikes occur when synapses are distributed in dendritic regions with a sublinearity of less than 20%, causing increased somatic maximum spike rate. With 400 synapses, CS can not be induced when synapses are distributed only in dendrites with sublinearity greater than 40%. When the input increases to 800 synapses, CSs occur more robustly and therefore the somatic maximum spike rate increases further. Overall, stronger sublinearity inhibits CS production. These results reveal the mechanism of bursting complex spikes highly depends on the dendritic sublinearity.

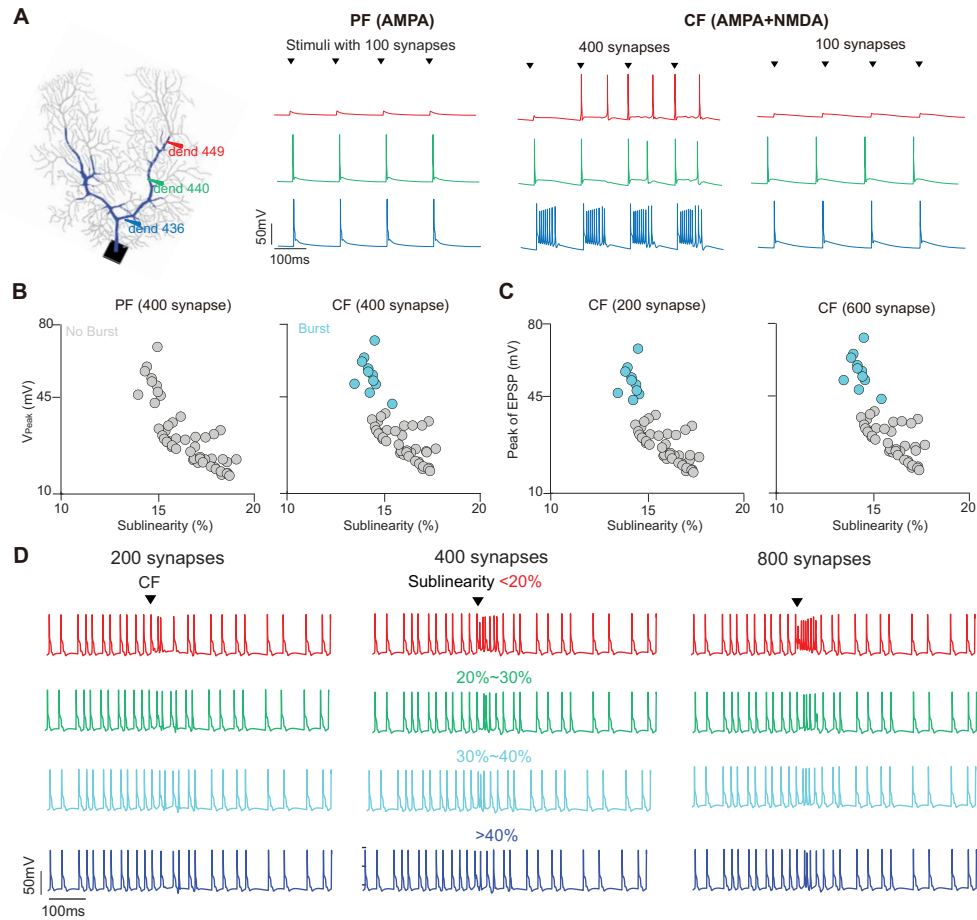


Fig. 6: Bursting complex spikes are suppressed by strong sublinearity. (A) 400 synapses cluster input in three dendrites. Somatic voltage responses triggered by each stimulation site with and without NMDARs. The triangle represents the time of stimulation. (B) Scatter plots showing the peak of EPSP and sublinearity of main dendrites with NMDA and without NMDA. Cyan scatter and dendrites indicated that somatic has a burst response. (C) Similar to B, but with 200 synapses (left) and 600 synapses (right) cluster input. (D) Strong sublinearity suppresses burst. PC installed with 1000 PF AMPA synapses stimulated at 30 Hz Poisson spikes and a CF with 200, 400 and 800 AMPA+NMDA synapses distributed on different sublinear dendrites.

D. Dendritic sublinearity implements the feature binding

We finally examine the functional role of dendritic sublinearity using classical computing tasks. Our PC model has 24 branches based on dendritic sublinearity, where each branch can be a single computing unit. We first consider the computing task of the Boolean function. For this, synapses are assigned with a binary value of 0 or 1. The final output is 1 if the PC fire spikes,

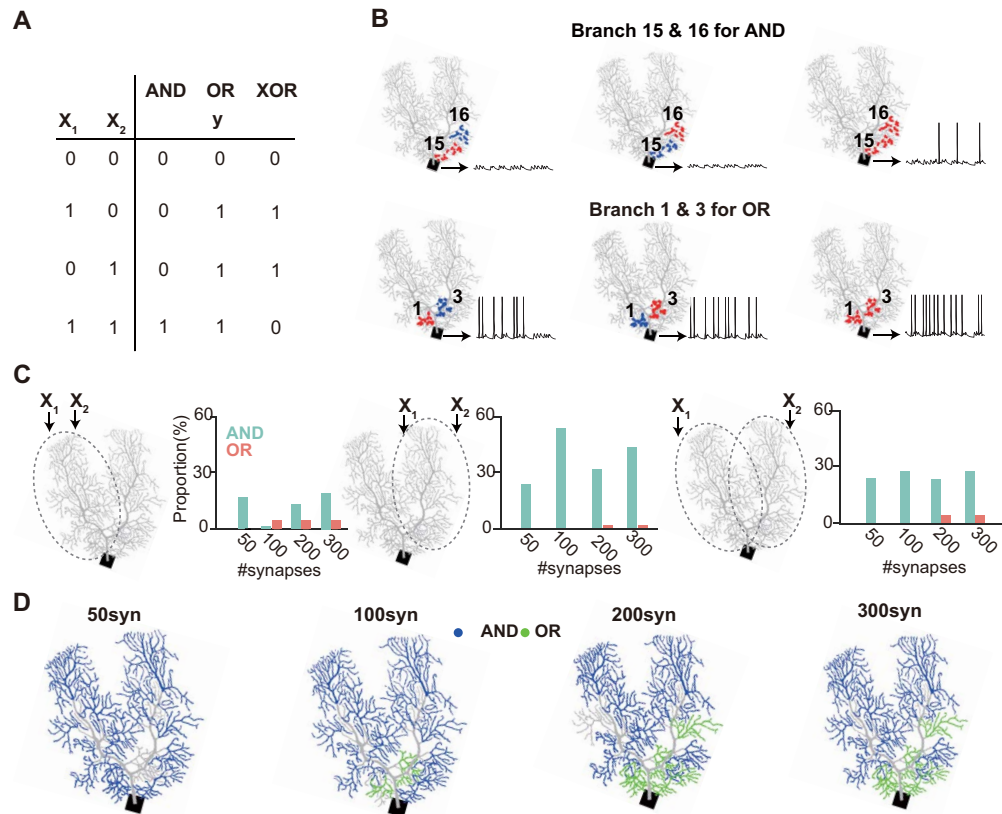


Fig. 7: Sublinear dendrites implement Boolean functions. (A) 24 branches with each representing a computing unit. Synapses are binary as 0 or 1 for the truth table of AND, OR, and XOR with two inputs (X_1 and X_2). (B) Branches 15 & 16 for AND, and branches 1 & 3 for OR. Colored dots indicate the distribution location of synapses, blue for inactivation, and red for activation. 100 synapses with 50 Hz synchronous input on each branch. (C) Two synchronous inputs on the left, right, and both the main branches. The bar chart shows the ratio of pairs of branches for AND and OR. (D) The distribution of branches participating in AND (blue) and OR (green) with different synapse inputs. Gray areas indicate regions not participating in any Boolean operations.

otherwise 0 for no spike. In this context the input-output relationship can be described by a unique truth table, corresponding to a Boolean function (Figure 7A). The truth table describes three simple Boolean functions: OR, AND, and XOR. To compute this, we applied synaptic inputs on a pair of branches, went through all the pairs out of 24 branches, and recorded the somatic membrane response (Figure 7B). Examples show that the neural model can implement either the AND (branches 15 and 16), or OR (branches 1 and 3) Boolean function. However, no

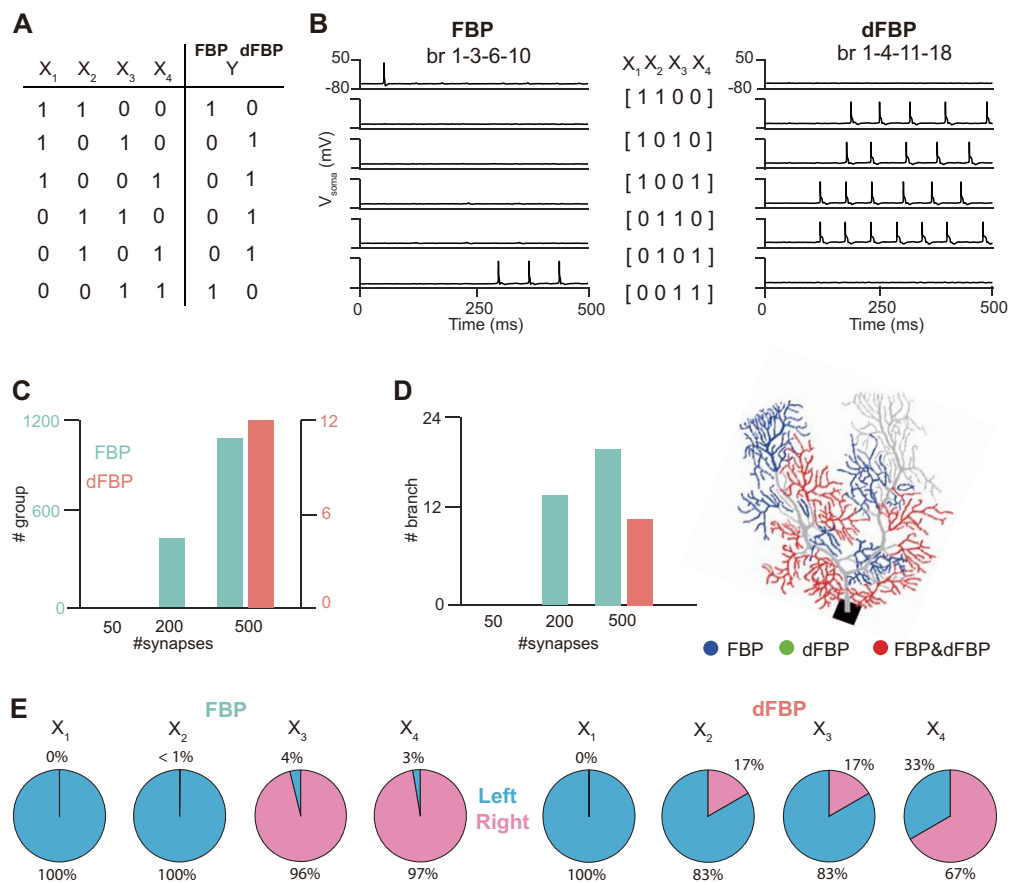


Fig. 8: Sublinear dendrites implement the feature binding problem (FBP) and dual feature binding problem (dFBP). (A) FBP and dFBP with 4 variables. (B) Examples of FBP and dFBP computed by a group of 4 branches. The somatic voltage trace in response to different input vectors where one active input variable is represented by an asynchronous input with 500 synapses at 50 Hz. (C) The number of branch ensembles (groups) for FBP and dFBP with an input of different numbers of synapses. (D) The number of branches for FBP and dFBP and their distribution on the dendritic tree. Blue regions indicate participation only in feature binding problem (FBP), green regions indicate participation only in double feature binding problem (dFBP), and red regions indicate participation in both FBP and dFBP. Gray areas indicate regions not participating in any feature binding operations. (E) The distribution of 4 input vectors on the left and right main branches when implementing FBP and dFBP.

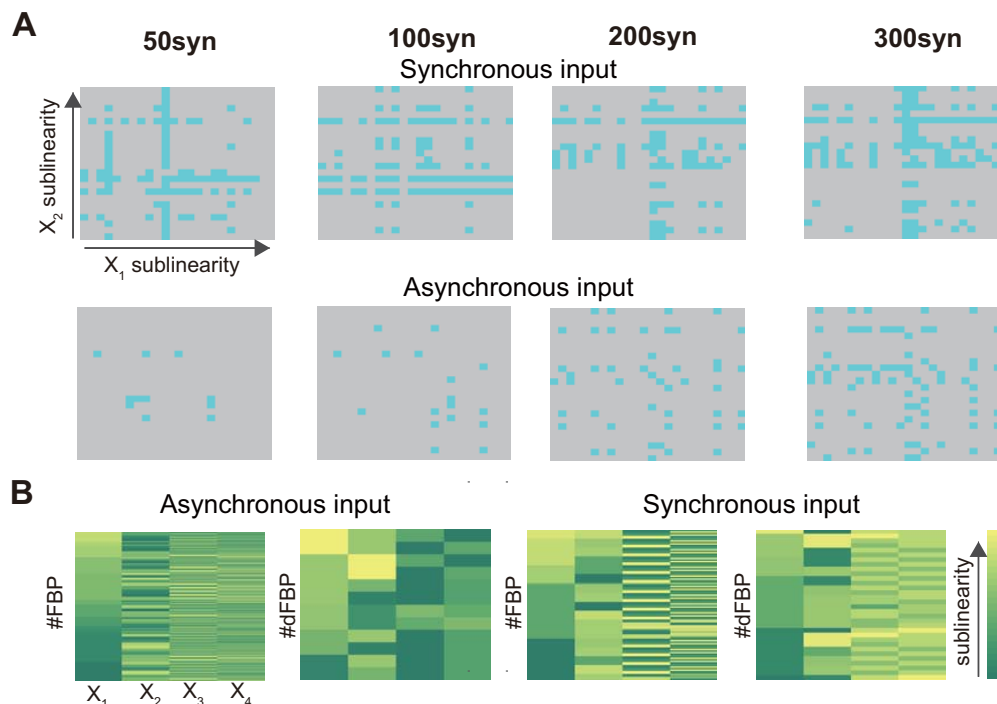


Fig. 9: (A) Schematic diagram illustrating the sorting of dendritic branch sublinearity indices (SI) and the implementation of AND operations (cyan) with different numbers of synapses (50, 100, 200, 300) under synchronous and asynchronous input conditions. In general, it is not easy to produce AND operations when the sublinearities of x_1 and x_2 are both weak. Higher sublinearity indices facilitate AND operations. (B) When executing FBP and dFBP, a schematic diagram of the sublinearity of the four branches.

example of XOR was found. The particular PC has two major trunk dendrites, so we exhausted all possible pairs on both trunks and counted the percentage of pairs for each Boolean function (Figure 7C). In the left main trunk, only AND can be performed when the number of synaptic inputs is 50, and the cell starts to perform OR as the number of synapses increases. At the right main trunk, the PC implements a higher proportion of ANDs and requires a higher number of synapses to perform OR. When the two branches are from the two main trunks, the change in the number of synapses has little effect on performing AND, while more difficult to implement OR. In general, the cell prefers to perform AND, and more synaptic inputs are required to perform OR with synchronous inputs (Figure 7D). Such observations are relatively independent of the temporal input protocols and preserved when asynchronous inputs were used (Supplemental

Figure S4).

We then consider a more difficult computing task of feature binding problem (FBP) [43]. For the input, we considered that the four input variables $X_i, i = 1, 2, 3, 4$ corresponded to four afferent neural ensembles of 500 neurons each in each branch, and that an ensemble was active, signaling $X_i = 1$. For the output, we considered a single somatic spike as the response to an input vector, such that if the neuron fires a spike then $Y = 1$, and no spike as $Y = 0$. Thus, to implement the FBP successfully, the cell should only fire spike in response to the input vectors $X = [1, 1, 0, 0], [0, 0, 1, 1]$, and not to spike for the remaining four input vectors (Figure 8A). The dual feature binding problem (dFBP) is the opposite. The neuron should not fire spikes in response to the input vectors $X = [1, 1, 0, 0], [0, 0, 1, 1]$, and only spike for the remaining four input vectors. Indeed, we found the neuron can implement FBP, for example, with a combination of branches 1, 3, 6, and 10 (Figure 8B, left), and dFBP with a combination of branches 1, 4, 11, and 18 (Figure 8B, right). Next, we want over 24 branches with a group of four branches for all input vectors and recorded the number of groups of branches for both FBP and dFBP tasks (Figure 8C) with asynchronous inputs. By varying the number of synaptic inputs, we found that implementing dFBP requires more inputs while FBP requires an appropriate number of synapses. As the number of synapses increases, the number of branches involved in the implementation of FBP increases. Compared to FBP, there are significantly fewer groups that can implement dFBP. Particularly, nearly all branches can be involved in FBP, while only half of the branches for dFBP over all 24 branches (Figure 8D). We analyzed how the branches involved in FBP and dFBP are distributed over the four input vectors, and found that X_1 and X_2 tend to sit in the one trunk and X_3 and X_4 on the other trunk (Figure 8E), due to that the two branches produce stronger sublinearity when they are on different main dendrites. For instance, the observed EPSP $O(\text{EPSP}_{\text{br1+br2}})$ will be smaller than the expected $E(\text{EPSP}_{\text{br1+br2}})$ when two branches on different main dendrites. Generally speaking, there is further sublinearity between different branch combinations. Such observations highly depend on the temporal input protocol. When synchronous input was used, dFBP was more easily implemented with fewer numbers of synaptic inputs (Supplemental Figure S5). In addition, the sublinearity index of each branch is calculated by the average of the sublinearity index of all dendrites within the branch (Supplemental Figure S6). From Figure 9A, it was observed that when inputs x_1 and x_2 are both distributed in branches with weak sublinearity, the neuron struggles to perform AND operations. However, the likelihood of achieving AND operations increases when at least

one of the inputs is distributed in a branch with moderate sublinearity. Additionally, achieving effective feature binding problem (FBP) and double feature binding problem (dFBP) requires a balance of sublinearity within the four branches, emphasizing the need for a moderate balance of sublinearity to support these complex computations Figure 9B.

IV. DISCUSSION

In the realm of single-neuron computation, the rational underpinning lies in the intricacies of nonlinear dendritic behavior. Here utilizing a Purkinje cell model with the detailed dendritic morphology, we revealed a distinctive feature of sublinear synaptic integration at different parts of dendrites. It is this inherent sublinearity within the dendritic architecture that empowers cerebellar PCs to implement binding of different features, potentially sending from parallel and climbing fibers. Our study sheds light on the computational prowess of PCs, emphasizing the pivotal role played by dendritic sublinearity in facilitating the realization of intricate neural computations.

A. *Sublinear dendritic integration in Purkinje cells*

Neurons within the cerebellum manifest intricate nonlinear properties, a phenomenon deemed critical in orchestrating network functionality [44]. The dendrites of cerebellar interneurons intricately filter synaptic response times and amplitudes, engendering sublinear input-output relationships. Elucidating the transformation of temporally and spatially distributed inputs from granular cells constitutes a crucial pursuit in understanding their operational dynamics [21], [22]. Notably, the morphological attributes of neurons introduce a consequential dimension, wherein the amplitude and configuration of local EPSPs are subject to the nuanced intricacies of neuronal form [45].

In stark contrast, PCs present a more intricate dendritic morphology, necessitating the integration of a greater multitude of synaptic inputs. Our investigation reveals a distinctive property: PC dendrites manifest sublinear synaptic integration, with the degree of sublinearity accentuated in thin dendrites as opposed to their thicker counterparts. Remarkably, this position-dependent nonlinearity in synaptic integration is reminiscent of observations in CA1 pyramidal neurons [11]. A plausible rationale lies in the elevated input resistance of thin dendrites, mitigating the driving forces for synaptic current flow concerning their thicker counterparts. This underlines the PC's ability to differentiate similar inputs based on the synaptic distribution position. Moreover,

the integration of inputs from granule cells, strategically distributed along the spiny dendrites, undergoes effective filtering to preclude saturation.

Intriguingly, PC dendrites exhibit sensitivity to synaptic inputs at the millisecond scale. This contrasts with pyramidal cell dendrites, which, within short temporal intervals (0–5 ms), exhibit either linearity or slight supralinearity [46], [47]. However, as temporal intervals extend (5–100 ms), EPSP summation in pyramidal cell dendrites becomes sublinear [48], [49]. The heightened sensitivity of PC dendrites to millisecond-scale synaptic information potentially accounts for the precise synchronous firing of simple spikes in on-beam Purkinje cells during cerebellar behaviors [50], [51], [52]. In addition, Purkinje cells control the coordination and adaptation of sensorimotor behavior during visuomotor behavior by nonlinearly integrating signals [53]. Nonlinearity allows Purkinje cells to respond sensitively to minute changes in input signals while maintaining a stable response across a broad range of input signal intensities. This means that Purkinje cells can precisely regulate the inhibitory signals they send to the deep nuclei of the cerebellum, thus finely controlling movement [54]. In concert, the observed sublinear integration in PCs assumes the role of an activity-dependent spatial filter, contributing substantively to the adaptive filter behavior within the cerebellar cortex.

B. Dendrites sublinearity affects neuronal input-output dynamics

The intricate interplay between theory and experimentation has consistently stressed the critical role played by dendrites in shaping the input-output neuronal dynamics, conferring formidable computing capabilities upon individual neurons [55], [14], [15], [4]. The influence of nonlinear dendritic integration in actively modulating neuronal responses has been experimentally demonstrated across diverse cortical areas [56], [57], [58]. Theoretical insights suggest that dendritic superlinearity renders neurons sensitive to clustering, while sublinearity engenders a sensitivity to scattering [31], [43].

Our findings unveil a distinctive characteristic of PC dendrites, wherein pronounced sublinearity translates into global scatter sensitivity, particularly in response to asynchronous inputs. This outcome suggests a resilience of PCs against firing induced by clustered granule cell inputs, attributed to the abundance and sparsity of granule cells, thus avoiding the triggering of PC firing by a limited subset of granule cells. Remarkably, in the somatosensory cortex, features are localized within single dendrites [59], while synapses in the visual and auditory cortex’s layer 2/3 pyramidal neurons exhibit maximal responsiveness to inputs carrying distinct

sensory features [60], [61]. Consequently, this global scatter strategy aligns with the neuron’s responsiveness to multi-feature discrete distributions. Furthermore, our investigation illuminates that weak sublinearity in dendrites favors the generation of bursts. Notably, the principal dendrite establishing a synaptic connection between climbing fibers and PC emerges as a region of weak sublinearity. This finding posits that climbing fiber inputs can more readily induce PCs to generate intricate complex spikes.

C. Dendritic nonlinearity implements feature binding

Should dendrites merely serve as collectors of input, performing linear summation at the soma, a single neuron would be confined to computing solely linearly separable input-output functions. However, experimental evidence has revealed the capacity of neuronal dendrites to undergo nonlinear synaptic integration [30], [23], [12], [8]. Neurons exhibiting the nonlinear synaptic integration transcend the limitation, calculating both linearly separable and non-separable functions. Theoretical investigations underscore the transformative role of dendritic nonlinearity, empowering individual neurons to execute linearly inseparable functions [62], [43], [31], [63], with recent experiments showcasing the capability of cerebellar stellate cells to solve feature binding problems [32].

In our study, we unveil the capability of PCs with sublinear dendritic characteristics, demonstrating their capacity to perform Boolean operations, primarily preferred AND operations. As the synaptic inputs increase, the execution of OR operations becomes more pronounced. Remarkably, the facilitation of AND operations is prominent when two inputs are strategically distributed on one of the two main trunk dendrites, however, the XOR operation is unachievable here, unlike human pyramidal cells [64]. Furthermore, the sublinear attributes of PC dendrites contribute to implementing feature binding problems, where both both asynchronous and synchronous input can realize dual feature binding problems. Intriguingly, during the implementation of the feature binding problem, inputs appear equally distributed among the main primary dendrites. This observation aligns with the notion that more primary dendrites are requisite for complex functions. Notably, human PCs [65], [66], characterized by more intricate dendritic structures and enhanced computing capabilities compared to rodents, typically exhibit 2-3 main trunks, in contrast to most rodents with only a single main trunk. The presence of multiple dendritic trunks is correlated with climbing fiber connections and long-term synaptic plasticity [67] and this innervation pattern can generate independent computational compartments within a single

Purkinje cell [66]. Our findings further propose that branches between main dendrites boost sublinear synaptic integration, thereby augmenting the computational capability of a single neuron. Together with other recent studies, neurons endowed with nonlinear dendritic characteristics surpass their linear counterparts in computing more complex tasks [27].

D. Limitation

Ion channel currents play a crucial role in shaping the integrated properties of neurons, exemplified by the currents through Na and Ca^2 channels. These currents serve to recompense synaptic currents lost through membrane resistance, thereby influencing the overall functionality of neurons [45]. Notably, the presence of dendritic spine $CaV_{2.3}$ voltage-sensitive calcium channels introduces a nonlinear regulatory mechanism for synaptic input within neurons [68]. PC dendrites exhibit an intricate distribution of ion channels, adding a layer of complexity to the nonlinear function [9], [69]. Moreover, Purkinje cells also receive inhibitory input from interneurons and significantly impact PC dynamics [70], which is essential for the precise timing and coordination of muscular activities controlled by the cerebellum [71], [72]. However, the effect of inhibitory input on the nonlinear synaptic integration ability of Purkinje cells has not been studied in depth here. However it is obvious that inhibition will further regulate the nonlinear synaptic integration ability of Purkinje cells, in particular, inhibitory strength depends on input location. Future research should investigate the impact of voltage-dependent ion channels and inhibitory input on dendritic nonlinearity to fully understand the complex mechanisms underpinning Purkinje cell function.

REFERENCES

- [1] J. T. Davie, M. H. Kole, J. J. Letzkus, E. A. Rancz, N. Spruston, G. J. Stuart, and M. Häusser, “Dendritic patch-clamp recording,” *Nature protocols*, vol. 1, no. 3, pp. 1235–1247, 2006.
- [2] N. Spruston, “Pyramidal neurons: dendritic structure and synaptic integration,” *Nature Reviews Neuroscience*, vol. 9, no. 3, pp. 206–221, 2008.
- [3] N. Spruston, G. Stuart, and M. Häusser, “Principles of dendritic integration,” *Dendrites*, vol. 351, no. 597, p. 1, 2016.
- [4] M. Lafourcade, M.-S. H. van der Goes, D. Vardalaki, N. J. Brown, J. Voigts, D. H. Yun, M. E. Kim, T. Ku, and M. T. Harnett, “Differential dendritic integration of long-range inputs in association cortex via subcellular changes in synaptic ampa-to-nmda receptor ratio,” *Neuron*, vol. 110, no. 9, pp. 1532–1546, 2022.
- [5] T. Branco and M. Häusser, “The single dendritic branch as a fundamental functional unit in the nervous system,” *Current opinion in neurobiology*, vol. 20, no. 4, pp. 494–502, 2010.
- [6] M. London and M. Häusser, “Dendritic computation,” *Annu. Rev. Neurosci.*, vol. 28, pp. 503–532, 2005.

- [7] C. Koch and I. Segev, "The role of single neurons in information processing," *Nature neuroscience*, vol. 3, no. 11, pp. 1171–1177, 2000.
- [8] P. Poirazi and A. Pappas, "Illuminating dendritic function with computational models," *Nature Reviews Neuroscience*, vol. 21, no. 6, pp. 303–321, 2020.
- [9] G. J. Stuart and N. Spruston, "Dendritic integration: 60 years of progress," *Nature neuroscience*, vol. 18, no. 12, pp. 1713–1721, 2015.
- [10] R. Makarov, M. Pagkalos, and P. Poirazi, "Dendrites and efficiency: Optimizing performance and resource utilization," *Current Opinion in Neurobiology*, vol. 83, p. 102812, 2023.
- [11] S. Cash and R. Yuste, "Linear summation of excitatory inputs by cal pyramidal neurons," *Neuron*, vol. 22, no. 2, pp. 383–394, 1999.
- [12] A. Polsky, B. W. Mel, and J. Schiller, "Computational subunits in thin dendrites of pyramidal cells," *Nature neuroscience*, vol. 7, no. 6, pp. 621–627, 2004.
- [13] M. E. Larkum, J. J. Zhu, and B. Sakmann, "A new cellular mechanism for coupling inputs arriving at different cortical layers," *Nature*, vol. 398, no. 6725, pp. 338–341, 1999.
- [14] T. Branco, B. A. Clark, and M. Häusser, "Dendritic discrimination of temporal input sequences in cortical neurons," *Science*, vol. 329, no. 5999, pp. 1671–1675, 2010.
- [15] G. Major, M. E. Larkum, and J. Schiller, "Active properties of neocortical pyramidal neuron dendrites," *Annual review of neuroscience*, vol. 36, pp. 1–24, 2013.
- [16] T. Branco and M. Häusser, "Synaptic integration gradients in single cortical pyramidal cell dendrites," *Neuron*, vol. 69, no. 5, pp. 885–892, 2011.
- [17] A. Losonczy and J. C. Magee, "Integrative properties of radial oblique dendrites in hippocampal cal pyramidal neurons," *Neuron*, vol. 50, no. 2, pp. 291–307, 2006.
- [18] S. Gasparini and J. C. Magee, "State-dependent dendritic computation in hippocampal cal pyramidal neurons," *Journal of Neuroscience*, vol. 26, no. 7, pp. 2088–2100, 2006.
- [19] H. Hu, M. Martina, and P. Jonas, "Dendritic mechanisms underlying rapid synaptic activation of fast-spiking hippocampal interneurons," *Science*, vol. 327, no. 5961, pp. 52–58, 2010.
- [20] A. G. Carter, G. J. Soler-Llavina, and B. L. Sabatini, "Timing and location of synaptic inputs determine modes of subthreshold integration in striatal medium spiny neurons," *Journal of Neuroscience*, vol. 27, no. 33, pp. 8967–8977, 2007.
- [21] T. Abrahamsson, L. Cathala, K. Matsui, R. Shigemoto, and D. A. DiGregorio, "Thin dendrites of cerebellar interneurons confer sublinear synaptic integration and a gradient of short-term plasticity," *Neuron*, vol. 73, no. 6, pp. 1159–1172, 2012.
- [22] A. Tran-Van-Minh, T. Abrahamsson, L. Cathala, and D. A. DiGregorio, "Differential dendritic integration of synaptic potentials and calcium in cerebellar interneurons," *Neuron*, vol. 91, no. 4, pp. 837–850, 2016.
- [23] N.-l. Xu, M. T. Harnett, S. R. Williams, D. Huber, D. H. O'Connor, K. Svoboda, and J. C. Magee, "Nonlinear dendritic integration of sensory and motor input during an active sensing task," *Nature*, vol. 492, no. 7428, pp. 247–251, 2012.
- [24] D. E. Wilson, D. E. Whitney, B. Scholl, and D. Fitzpatrick, "Orientation selectivity and the functional clustering of synaptic inputs in primary visual cortex," *Nature neuroscience*, vol. 19, no. 8, pp. 1003–1009, 2016.
- [25] N. Takahashi, T. G. Oertner, P. Hegemann, and M. E. Larkum, "Active cortical dendrites modulate perception," *Science*, vol. 354, no. 6319, pp. 1587–1590, 2016.
- [26] M. Lavzin, S. Rapoport, A. Polsky, L. Garion, and J. Schiller, "Nonlinear dendritic processing determines angular tuning of barrel cortex neurons in vivo," *Nature*, vol. 490, no. 7420, pp. 397–401, 2012.

- [27] P. Kaifosh and A. Losonczy, “Mnemonic functions for nonlinear dendritic integration in hippocampal pyramidal circuits,” *Neuron*, vol. 90, no. 3, pp. 622–634, 2016.
- [28] A. Tzilivaki, G. Kastellakis, and P. Poirazi, “Challenging the point neuron dogma: Fs basket cells as 2-stage nonlinear integrators,” *Nature communications*, vol. 10, no. 1, p. 3664, 2019.
- [29] Y. Katz, V. Menon, D. A. Nicholson, Y. Geinisman, W. L. Kath, and N. Spruston, “Synapse distribution suggests a two-stage model of dendritic integration in ca1 pyramidal neurons,” *Neuron*, vol. 63, no. 2, pp. 171–177, 2009.
- [30] C. Koch, T. Poggio, and V. Torre, “Nonlinear interactions in a dendritic tree: localization, timing, and role in information processing,” *Proceedings of the National Academy of Sciences*, vol. 80, no. 9, pp. 2799–2802, 1983.
- [31] R. D. Cazé, M. Humphries, and B. Gutkin, “Passive dendrites enable single neurons to compute linearly non-separable functions,” *PLoS computational biology*, vol. 9, no. 2, p. e1002867, 2013.
- [32] R. D. Cazé, A. Tran-Van-Minh, B. S. Gutkin, and D. A. DiGregorio, “Demonstration that sublinear dendrites enable linearly non-separable computations,” *bioRxiv*, pp. 2023–06, 2023.
- [33] P. Poirazi, T. Brannon, and B. W. Mel, “Pyramidal neuron as two-layer neural network,” *Neuron*, vol. 37, no. 6, pp. 989–999, 2003.
- [34] D. Beniaguev, I. Segev, and M. London, “Single cortical neurons as deep artificial neural networks,” *Neuron*, vol. 109, no. 17, pp. 2727–2739, 2021.
- [35] X. Li, J. Tang, Q. Zhang, B. Gao, J. J. Yang, S. Song, W. Wu, W. Zhang, P. Yao, N. Deng *et al.*, “Power-efficient neural network with artificial dendrites,” *Nature Nanotechnology*, vol. 15, no. 9, pp. 776–782, 2020.
- [36] S. Chavlis and P. Poirazi, “Drawing inspiration from biological dendrites to empower artificial neural networks,” *Current opinion in neurobiology*, vol. 70, pp. 1–10, 2021.
- [37] X. Wu, P. Zhao, Z. Yu, L. Ma, K.-W. Yip, H. Tang, G. Pan, and T. Huang, “Mitigating communication costs in neural networks: The role of dendritic nonlinearity,” *arXiv preprint arXiv:2306.11950*, 2023.
- [38] A. Galakhova, S. Hunt, R. Wilbers, D. Heyer, C. de Kock, H. Mansvelder, and N. Goriounova, “Evolution of cortical neurons supporting human cognition,” *Trends in Cognitive Sciences*, vol. 26, no. 11, pp. 909–922, 2022.
- [39] R. Napper and R. Harvey, “Number of parallel fiber synapses on an individual purkinje cell in the cerebellum of the rat,” *Journal of Comparative Neurology*, vol. 274, no. 2, pp. 168–177, 1988.
- [40] M. Watanabe and M. Kano, “Climbing fiber synapse elimination in cerebellar purkinje cells,” *European Journal of Neuroscience*, vol. 34, no. 10, pp. 1697–1710, 2011.
- [41] Y. Tang, X. Zhang, L. An, Z. Yu, and J. K. Liu, “Diverse role of nmda receptors for dendritic integration of neural dynamics,” *PLOS Computational Biology*, vol. 19, no. 4, p. e1011019, 2023.
- [42] J. S. Rothman, L. Cathala, V. Steuber, and R. A. Silver, “Synaptic depression enables neuronal gain control,” *Nature*, vol. 457, no. 7232, pp. 1015–1018, 2009.
- [43] A. Tran-Van-Minh, R. D. Cazé, T. Abrahamsson, L. Cathala, B. S. Gutkin, and D. A. DiGregorio, “Contribution of sublinear and supralinear dendritic integration to neuronal computations,” *Frontiers in cellular neuroscience*, vol. 9, p. 67, 2015.
- [44] E. D’Angelo, “Physiology of the cerebellum,” *Handbook of clinical neurology*, vol. 154, pp. 85–108, 2018.
- [45] J. C. Magee, “Dendritic integration of excitatory synaptic input,” *Nature Reviews Neuroscience*, vol. 1, no. 3, pp. 181–190, 2000.
- [46] J. Schiller, G. Major, H. J. Koester, and Y. Schiller, “Nmda spikes in basal dendrites of cortical pyramidal neurons,” *Nature*, vol. 404, no. 6775, pp. 285–289, 2000.
- [47] N. N. Urban and G. Barrionuevo, “Active summation of excitatory postsynaptic potentials in hippocampal ca3 pyramidal neurons,” *Proceedings of the National Academy of Sciences*, vol. 95, no. 19, pp. 11 450–11 455, 1998.

- [48] J. C. Magee, “Dendritic Ih normalizes temporal summation in hippocampal CA1 neurons,” *Nature neuroscience*, vol. 2, no. 6, pp. 508–514, 1999.
- [49] M. Margulis and C.-M. Tang, “Temporal integration can readily switch between sublinear and supralinear summation,” *Journal of neurophysiology*, vol. 79, no. 5, pp. 2809–2813, 1998.
- [50] C. de Solages, G. Szapiro, N. Brunel, V. Hakim, P. Isope, P. Buisseret, C. Rousseau, B. Barbour, and C. Lena, “High-frequency organization and synchrony of activity in the purkinje cell layer of the cerebellum,” *Neuron*, vol. 58, no. 5, pp. 775–788, 2008.
- [51] D. Heck, W. Thach, and J. Keating, “On-beam synchrony in the cerebellum as the mechanism for the timing and coordination of movement,” *Proceedings of the National Academy of Sciences*, vol. 104, no. 18, pp. 7658–7663, 2007.
- [52] A. L. Person and I. M. Raman, “Purkinje neuron synchrony elicits time-locked spiking in the cerebellar nuclei,” *Nature*, vol. 481, no. 7382, pp. 502–505, 2012.
- [53] L. D. Knogler, A. M. Kist, and R. Portugues, “Motor context dominates output from purkinje cell functional regions during reflexive visuomotor behaviours,” *Elife*, vol. 8, p. e42138, 2019.
- [54] S. A. Heiney, J. Kim, G. J. Augustine, and J. F. Medina, “Precise control of movement kinematics by optogenetic inhibition of purkinje cell activity,” *Journal of Neuroscience*, vol. 34, no. 6, pp. 2321–2330, 2014.
- [55] M. E. Larkum, T. Nevian, M. Sandler, A. Polsky, and J. Schiller, “Synaptic integration in tuft dendrites of layer 5 pyramidal neurons: a new unifying principle,” *Science*, vol. 325, no. 5941, pp. 756–760, 2009.
- [56] C. Grienberger, X. Chen, and A. Konnerth, “NMDA receptor-dependent multidendrite Ca²⁺ spikes required for hippocampal burst firing in vivo,” *Neuron*, vol. 81, no. 6, pp. 1274–1281, 2014.
- [57] S. L. Smith, I. T. Smith, T. Branco, and M. Häusser, “Dendritic spikes enhance stimulus selectivity in cortical neurons in vivo,” *Nature*, vol. 503, no. 7474, pp. 115–120, 2013.
- [58] L. M. Palmer, A. S. Shai, J. E. Reeve, H. L. Anderson, O. Paulsen, and M. E. Larkum, “NMDA spikes enhance action potential generation during sensory input,” *Nature neuroscience*, vol. 17, no. 3, pp. 383–390, 2014.
- [59] N. Takahashi, K. Kitamura, N. Matsuo, M. Mayford, M. Kano, N. Matsuki, and Y. Ikegaya, “Locally synchronized synaptic inputs,” *Science*, vol. 335, no. 6066, pp. 353–356, 2012.
- [60] H. Jia, N. L. Rochefort, X. Chen, and A. Konnerth, “Dendritic organization of sensory input to cortical neurons in vivo,” *Nature*, vol. 464, no. 7293, pp. 1307–1312, 2010.
- [61] X. Chen, U. Leischner, N. L. Rochefort, I. Nelken, and A. Konnerth, “Functional mapping of single spines in cortical neurons in vivo,” *Nature*, vol. 475, no. 7357, pp. 501–505, 2011.
- [62] R. Cazé, M. Humphries, and B. Gutkin, “Spiking and saturating dendrites differentially expand single neuron computation capacity,” *Advances in neural information processing systems*, vol. 25, 2012.
- [63] R. D. Cazé, “All neurons can perform linearly non-separable computations,” *F1000Research*, vol. 10, 2021.
- [64] A. Gidon, T. A. Zolnik, P. Fidzinski, F. Bolduan, A. Papoutsi, P. Poirazi, M. Holtkamp, I. Vida, and M. E. Larkum, “Dendritic action potentials and computation in human layer 2/3 cortical neurons,” *Science*, vol. 367, no. 6473, pp. 83–87, 2020.
- [65] S. Masoli, D. Sanchez-Ponce, N. Vrieler, K. Abu-Haya, V. Lerner, T. Shahar, H. Nedelescu, M. F. Rizza, R. Benavides-Piccione, J. DeFelipe *et al.*, “Human outperform mouse purkinje cells in dendritic complexity and computational capacity,” *bioRxiv*, pp. 2023–03, 2023.
- [66] S. E. Busch and C. Hansel, “Climbing fiber multi-innervation of mouse purkinje dendrites with arborization common to human,” *Science*, vol. 381, no. 6656, pp. 420–427, 2023.
- [67] F. Najafi and J. F. Medina, “Beyond “all-or-nothing” climbing fibers: graded representation of teaching signals in purkinje cells,” *Frontiers in neural circuits*, vol. 7, p. 115, 2013.

- [68] B. L. Bloodgood and B. L. Sabatini, “Nonlinear regulation of unitary synaptic signals by cav2.3 voltage-sensitive calcium channels located in dendritic spines,” *Neuron*, vol. 53, no. 2, pp. 249–260, 2007.
- [69] E. De Schutter and J. M. Bower, “An active membrane model of the cerebellar purkinje cell. i. simulation of current clamps in slice,” *Journal of neurophysiology*, vol. 71, no. 1, pp. 375–400, 1994.
- [70] Y. Tang, L. An, Y. Yuan, Q. Pei, Q. Wang, and J. K. Liu, “Modulation of the dynamics of cerebellar purkinje cells through the interaction of excitatory and inhibitory feedforward pathways,” *PLoS computational biology*, vol. 17, no. 2, p. e1008670, 2021.
- [71] C. Pouzat and S. Hestrin, “Developmental regulation of basket/stellate cell→ purkinje cell synapses in the cerebellum,” *Journal of Neuroscience*, vol. 17, no. 23, pp. 9104–9112, 1997.
- [72] M. J. Dizon and K. Khodakhah, “The role of interneurons in shaping purkinje cell responses in the cerebellar cortex,” *Journal of Neuroscience*, vol. 31, no. 29, pp. 10463–10473, 2011.

Supplemental Materials:

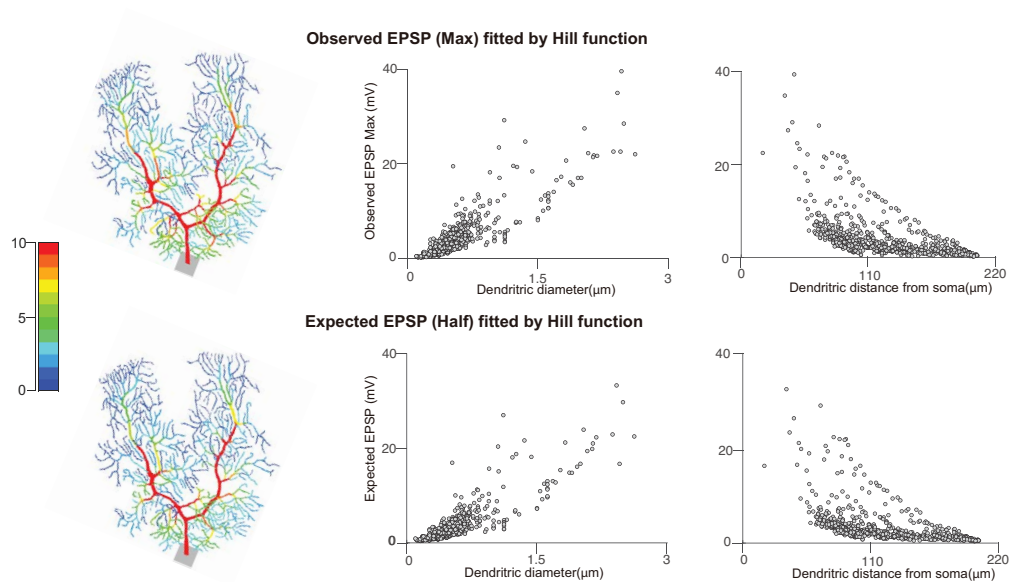


Fig. S1: Related to Figure 1. Color-coded (Top) the maximum observed EPSP (Max) and (Bottom) the value of expected EPSP at which observed EPSP reaches half maximum (Half) obtained by Hill function fits. Max and Half EPSP (Observed: Top, Expected: Bottom) as a function of dendritic diameter and distance from soma.

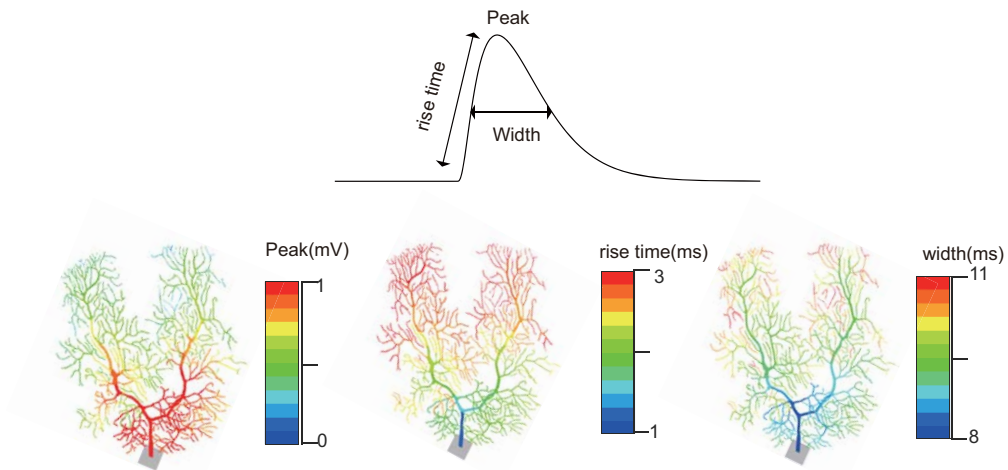


Fig. S2: Related to Figure1. The top panel illustrates the key parameters of an electrical signal: peak amplitude, rise time, and width of EPSP when a single synapse is distributed on different dendrites. The bottom panels display heatmaps of dendritic branches, visualizing the distribution of these parameters. From left to right, the maps show: Peak amplitude (mV), Rise time (ms) and width (ms). Color scales indicate the value ranges for each parameter, with red representing higher values and blue representing lower values. This visualization highlights the spatial variability of signal properties across the dendritic tree.

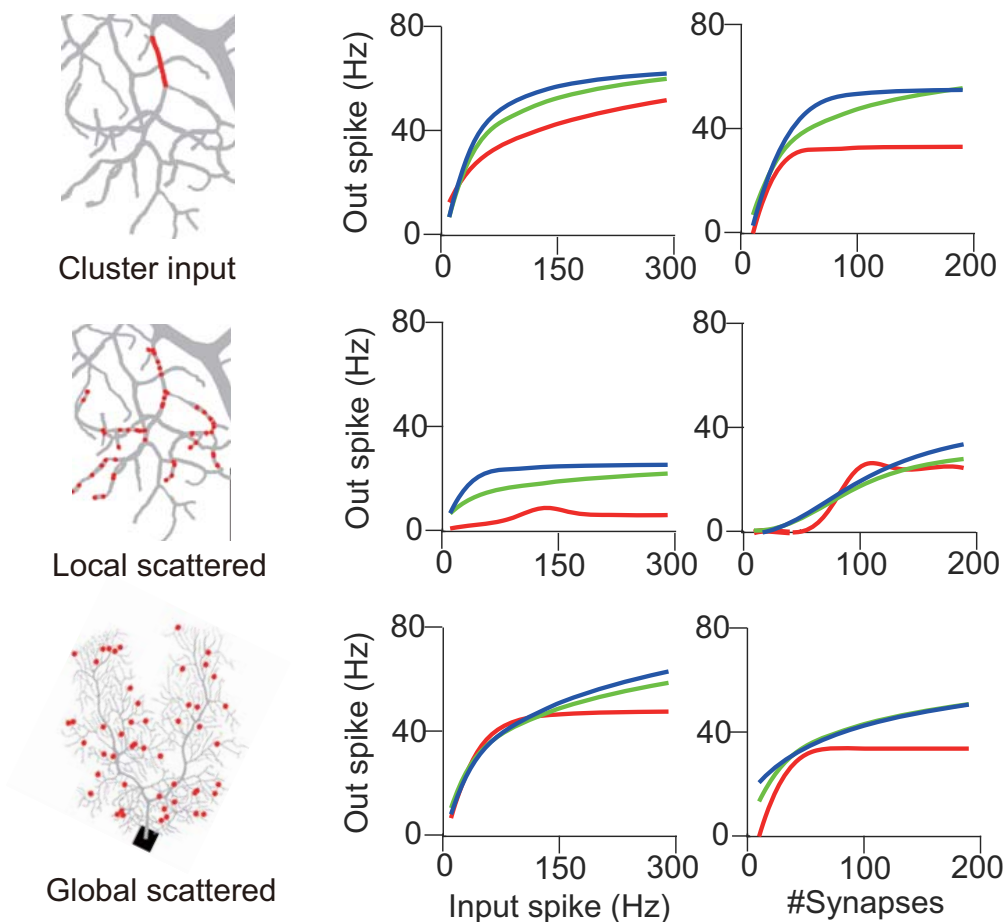


Fig. S3: Related to Figure4. Left column: Diagrams of three synaptic input distribution patterns: Cluster Input: Synapses concentrated in a single dendrite. Local Scattered: Synapses distributed across a branch area. Global Scattered: Synapses spread across the entire dendritic tree. Middle column: Output spike frequency (Hz) as a function of input spike frequency (Hz) with different numbers of synapses (50: red, 100: green, 150: blue). Right column: Output spike frequency (Hz) as a function of input spike frequency (Hz) with different input rate (50 Hz: red, 100 Hz: green, 150 Hz: blue). Here is synchronous input.

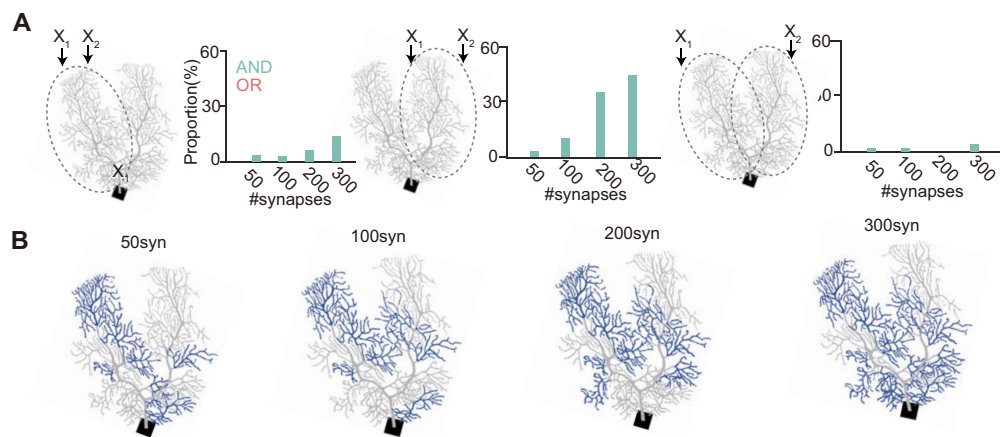


Fig. S4: Related to Figure7. (A) The proportion of AND and OR computations with varying numbers of synapses (50, 100, 200, 300) distributed on the left, right, and both the main branches with asynchronous inputs at 50Hz. (B) The distribution of branches participating in AND (blue) and OR (green) with different synapse inputs (50, 100, 200, 300). Gray areas indicate regions not participating in any Boolean operations.

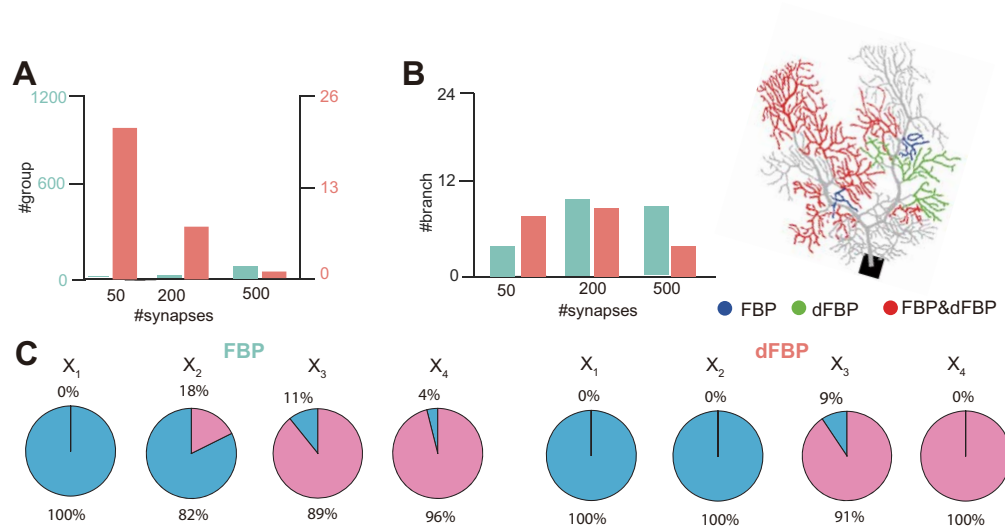


Fig. S5: Related to Figure8. (A) The number of branch ensembles (groups) for FBP and dFBP with an input of different numbers of synapses (20, 200, 500) with synchronous input at 50Hz. (B) The number of branches for FBP and dFBP and their distribution on the dendritic tree. Blue regions indicate participation only in feature binding problem (FBP), green regions indicate participation only in double feature binding problem (dFBP), and red regions indicate participation in both FBP and dFBP. Gray areas indicate regions not participating in any feature binding operations. (C) The distribution of 4 input vectors on the left and right main branches when implementing FBP and dFBP.

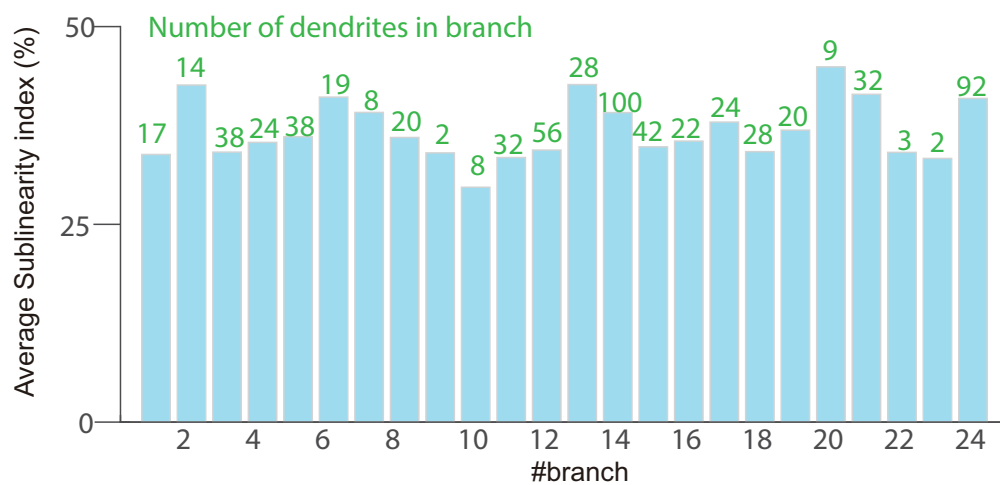


Fig. S6: Related to Figure9. The bar chart shows the average sublinearity index (%) for each dendritic branch. The green numbers above each bar indicate the number of dendrites in each branch. The sublinearity index reflects the degree of sublinear integration occurring in each branch, with higher values indicating greater sublinear integration. This data illustrates the variability in sublinear integration across different dendritic branches.